Acta Oceanol. Sin., 2016, Vol. 35, No. 5, P. 66–72
DOI: 10.1007/s13131-016-0848-3
http://www.hyxb.org.cn
E-mail: hyxbe@263.net

The improved model of estimating global whitecap coverage based on satellite data

REN Danqin[1], HUA Feng[1], YANG Yongzeng[1]*, SUN Baonan[1]

[1] First Institute of Oceanography, State Oceanic Administration, Qingdao 266061, China

Received 15 May 2015; accepted 20 August 2015

Abstract

The pro and con of whitecap parameterizations and a statistical wave breaking model are discussed. An improved model is derived by combining satellite-based parameterization and the wave breaking model. The appropriate constants for the general wave state are obtained by considering the breaking condition of the wave slope and fitting with the satellite-based parameterization. The result is close to the constants based on the whitecap data from Monahan. Comparing with satellite-based data and the original model's results, the improved model's results are consistent with satellite-based data and previous studies. The global seasonal distributions of the whitecap coverage averaged from 1998 to 2008 are presented. Spatial and seasonal features of the whitecap coverage are analyzed.

Key words: whitecap coverage, statistical wave breaking model, satellite-based parameterization

Citation: Ren Danqin, Hua Feng, Yang Yongzeng, Sun Baonan. 2016. The improved model of estimating global whitecap coverage based on satellite data. Acta Oceanologica Sinica, 35(5): 66–72, doi: 10.1007/s13131-016-0848-3

1 Introduction

Breaking waves in the ocean entrain air into sea water and form foamy patches on the sea surface and bubbles beneath. The fraction of the ocean surface mixed with bubbles and covered with sea foam is defined as the whitecap coverage (or foam fraction) W. They enhance air-sea exchange, leading to the physical processes different from those operating at the bubble-free water surface. Their surface extent provides a proxy measure for chemical and physical processes that are dependent upon bubbles and wave breaking, such as gas exchange (Monahan and Spillane, 1984; Asher et al., 1996; Woolf, 2005; Zhang, 2012), and sea spray aerosol production (Blanchard, 1963; de Leeuw et al., 2011).

Oceanic whitecap is one of the most important phenomena for wave breaking. It has been measured in field observations by many researchers and many empirical equations which are commonly parameterized as a function of local wind speed at a 10 m reference height U_{10}. These approaches ignore the known variability in the whitecap coverage resulting from the influence of factors such as the wave state, atmospheric stability and sea surface temperature (SST) (Monahan and O'Muircheartaigh, 1986; Anguelova and Webster, 2006; de Leeuw et al., 2011; Salisbury et al., 2013). Moreover, large gaps can be found among different empirical curves of whitecap coverage versus wind speed (Anguelova and Webster, 2006). So these approaches cannot satisfactorily describe the whitecap coverage.

Wave breaking is basically the intrinsic property of wind waves. The whitecap coverage observation with wind fetch clearly shows that longer fetch produces more whitecaps (Monahan, 1971; Stramska and Petelski, 2003). So sea wave characteristics should be considered for estimating whitecap coverage. The analytic expressions of whitecap coverage involved with both sea wave characteristics, and surface wind velocity have been derived in the statistical wave breaking model (Yuan et al., 2009).

However, the whitecap coverage estimated by the model is larger than the observed data. The concept, which choosing only two point of high wind speed on the upper envelope for all the whitecap coverage data derives the constants, may not be appropriate. So the paper is dedicated to combining empirical curve of whitecap coverage with the statistical wave breaking model, in improving the model. In Section 2, parameterized empirical equations are compared and analyzed. In Section 3, the whitecap coverage equation in the statistical wave breaking model and the approach of deriving the constants is introduced. In Section 4, the appropriate constants are determined and validated. Moreover, the global seasonal whitecap coverage is analyzed.

2 Whitecap coverage parameterizations

2.1 *Previous parameterizations*

Some researchers hold the point of view that wind speed is the main cause for wave breaking and the formation of whitecaps. They have proposed various empirical expressions of whitecap coverage versus wind velocity, each developed as the best fit to data set at specific locations and conditions. Nearly all of these relationships are expressed as a power law of the form:

$$W = a\,(U_{10} - b)^c\,, \tag{1}$$

where W is the sea surface whitecap coverage, U_{10} is the wind velocity at 10 m above the sea surface; and a, b and c are the fitting

Foundation item: The National Key Basic Research Program (973 Program) of China under contract No.2010CB950404; the National High Technology Research and Development Program (863 Program) of China under contract No.2013AA09A506; the Basic Scientific Fund for National Public Research Institutes of China under contract No.GY0214G01; the Ocean Renewable Energy Special Fund Project of the State Oceanic Administration of China under contract No.GHME2011ZC07.

*Corresponding author, E-mail: yangyz@fio.org.cn

coefficients. Previous wind speed parameterizations of whitecap fraction between 1963 and 2013 are summarized in Table 1 and plotted in Fig. 1.

Although this form of $W(U_{10})$ conforms to Cardone's (1969) and Monahan's (1971) suggestion that whitecaps manifest the dissipation of excessive energy transferred from the air flow to

Table 1. Parameterizations of whitecap coverage as a function of Eq. (1) between 1963 and 2013

Description	Condition	$a/10^{-5}$	b	c	Reference
Blanchard-1963	U_{10}>5 m/s (W=0, for U_{10} <3 m/s), supposing wind stress proportional to W	44	0	2	Blanchard (1963)
Monahan-1971	4 m/s <U_{10}⩽10 m/s, North Atlantic Ocean, 1968–1969 (May, July, August)	1.35	0	3.4	Monahan (1971)
M&O'M-1980-OLS	ordinary least squares fitting (OLS)	0.295	0	3.52	Monahan and O'Muircheartaigh (1980)
M&O'M-1980-RBF	robust biweight fitting (RBF)	0.384	0	3.41	Monahan and O'Muircheartaigh (1980)
M&O'M-1986*	considering the influence of stability, $W=a(U_{10}-b)c\mathrm{e}^{0.086\,1\Delta T}$	1.95	0	2.55	Monahan and O'Muircheartaigh (1986)
Wu-1988	in the Atlantic Ocean	0.17	0	3.75	Wu (1988)
M&W-1989-Y*	young stage, $W=a(U_{10}-b)c\mathrm{e}^{0.198\Delta T}$	0.029 2	0	3.204	Monahan and Woolf (1989)
M&W-1989-M*	mature stage, $W=a(U_{10}-b)c\mathrm{e}^{0.086\,1\Delta T}$	1.95	0	2.55	Monahan and Woolf (1989)
Wang-1990-W	whitecap	1.53	0	2.98	Wang et al. (1990)
Wang-1990-F	foam	1.65	0	3.29	Wang et al. (1990)
A&W-1998	on Georges Bank, April 8 to 17, 1990. SST approximately being 5.5°C depthapproximately being (35.4±1.7) m	0.256	–1.77	3	Asher and Wanninkhof (1998)
H&P-1999-Exc	exclude measurement W<5×10^{-5}	0.020 4	0	3.61	Hanson and Phillips (1999)
H&P-1999-All	all measurement considered	0.000 366	0	5.16	Hanson and Phillips (1999)
S&P-2003-All	all W measured. Summer seasons from 1998 to 2000 in the North Atlantic	4.18	–4.93	3	Stramska and Petelski (2003)
S&P-2003-Dev	developed sea (H_s >0.5 m)	5.0	–4.47	3	Stramska and Petelski (2003)
S&P-2003-Und	undeveloped sea (else)	8.75	–6.33	3	Stramska and Petelski (2003)
Villarino-2003-Sta	air-sea temperature difference is moderate, and the atmosphere is stable	0.232	0	3.499	Villarino et al. (2003)
Villarino-2003-Uns	unstable. North Mediterranean Sea	0.043	0	3.682	Villarino et al. (2003)
Callaghan-2008-Low	3.7 m/s <U_{10}⩽11.25 m/s. North East Atlantic. From June 11 to July 5, 2006	318	–3.7	3	Callaghan et al. (2008)
Callaghan-2008-Hig	9.25 m/s <U_{10}⩽23.09 m/s	48.2	1.98	3	Callaghan et al. (2008)
Goddijn-2011	North Atlantic, 2006.6. QuikSCAT	11.50	0	1.86	Goddijn-Murphy et al. (2011)
Salisbury-2013-F10	10 GHz, horizontal polarization. globe	4.6	0	2.26	Salisbury et al. (2013)
Salisbury-2013-F37	37 GHz, horizontal polarization	39.7	0	1.59	Salisbury et al. (2013)

Note: The formation of whitecaps is $W = a(U_{10}-b)^c$ except of the part marked with asterisk "*"; ΔT is near-water air stability.

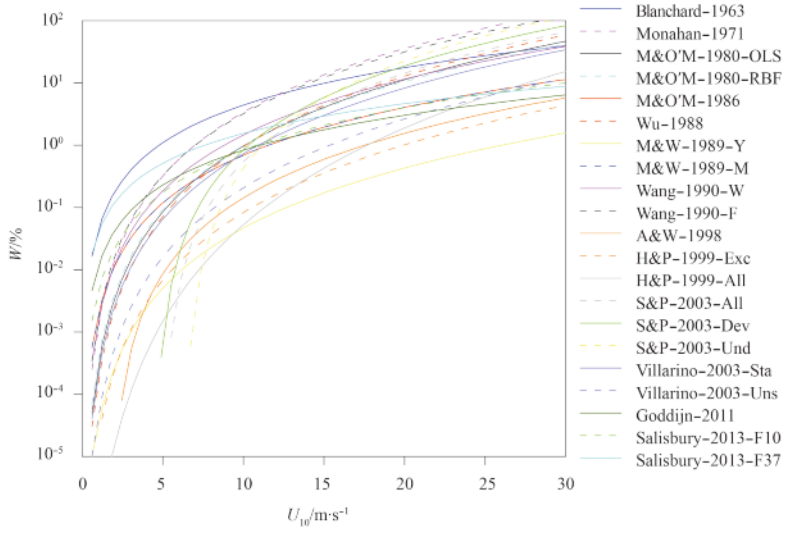

Fig. 1. Parameterizations of whitecap coverage between 1963 and 2013. The detailed descriptions of the legend are shown in Table 1.

the waves, these parameterizations in Fig. 1 have large variation in estimates of whitecap coverage, spanning several orders of magnitude. In Table 1 we can see that a ranges from 3.66×10^{-9} (Hanson and Phillips, 1999) to 3.18×10^{-3} (Callaghan et al., 2008), b ranges from 1.59 (Salisbury et al., 2013) to 5.16 (Hanson and Phillips, 1999) and c is from –6.33 (Stramska and Petelski, 2003) to 1.98 (Callaghan et al., 2008). Different values for a, b or c are related to different water temperatures, atmospheric stability, wind fetch and duration regimes.

Part of the variation is likely due to differences in both wind speed measurement methods and whitecap observation methods. Conditions encountered between different measurement campaigns also show large variation. Analysis of an insufficient number of images can lead to non-convergent W estimates with larger uncertainties and contribute to data scatter (Callaghan and White, 2009). Moreover, at different locations in the world ocean various environmental and meteorological factors act in concert but with different strengths and form a composite effect that either enhances or suppresses the effect of wind alone. So there is not sufficient documentation of different conditions to make a reliable comparison between data sets. Parameterization obtained by observations in a specified space and time is not suitable for other cases.

2.2 *Global measurement of whitecap*

Microwave radiometry, which can indirectly obtain consistent, long-term and global whitecap data, is a well-developed remote sensing technique that uses the natural emissivity of the ocean surface in its various states, such as large scale waves, smooth and roughened by small, and covered with sea foam (Ulaby et al., 1981). Furthermore, thorough study of the variability in whitecap is now viable with accompanying measurements of many different variables.

Whitecap estimates have been obtained by running the $W(T_B)$ algorithm (Anguelova and Webster, 2006). T_B is the brightness temperature in connection with ocean surface emissivity. The whitecap data consists of global whitecap values at two microwave frequencies, 10 GHz and 37 GHz (W_{10} and W_{37}) for horizontal polarization. Recent work on the electromagnetic properties of the sea foam, including the penetration depth of different microwave frequencies through sea foam (Anguelova and Gaiser, 2011), shows that each radiometric frequency has a different sensitivity to different stages of the whitecap. The sensitivity to thinner foam decreases with the frequency decreasing. The lower limit of detectable foam thickness for 37 GHz is around 1 mm, and for 10 GHz it is 4 mm. Thick foam is associated with the active whitecaps while thin foam characterizes residual whitecaps (Anguelova and Gaiser, 2011). So W estimates at 10 GHz can predominantly be representative of active stage of whitecaps, and at 37 GHz, W estimates can represent total whitecaps, namely active and residual stage of whitecaps (Salisbury et al., 2013).

Moreover, the satellite-based estimates of W are matched in space and time with six oceanographic and meteorological variables: wind speed U_{10}, wind direction U_{dir}, SST, air temperature T_a, significant wave height H_s and peak wave period T_p.

W_{10} and W_{37} can be parameterized as functions of wind speed by a fitting power law to the bin means (Salisbury et al., 2013):

$$W_{10} = 4.60\times10^{-3}U_{10}^{2.26}\ \ (2\,\mathrm{m/s} < U_{10} \leqslant 20\,\mathrm{m/s})\,. \tag{2}$$

$$W_{37} = 3.97\times10^{-2}U_{10}^{1.59}\ \ (2\,\mathrm{m/s} < U_{10} \leqslant 20\,\mathrm{m/s})\,. \tag{3}$$

W is expressed in percent. Although these parameterizations are in terms of U_{10} alone, they carry information for the variations of whitecaps because Eqs (2) and (3) are based on W data covering meteorological and oceanographic conditions over the entire globe over a full year.

3 Whitecap estimates by the statistical wave breaking model

3.1 *Introduction for the analytical solution of whitecap*

The statistical model for wave breaking is based on surface wave dynamics (Yuan et al., 2009). The expression of whitecap is derived by using breaking entrainment depth h_{en} and breaking area S_t as

$$\begin{aligned} W &= \int_0^{T_{en}} S_t f\left(\frac{t}{T_{en}}\right)\mathrm{d}t = \int_0^1 T_{en}S_t f\left(\frac{t}{T_{en}}\right)\mathrm{d}\left(\frac{t}{T_{en}}\right) \\ &= F_T\frac{h_{en}}{U_B}S_t, \end{aligned} \tag{4}$$

where

$$F_T = \int_0^1 f\left(\frac{t}{T_{en}}\right)\mathrm{d}\left(\frac{t}{T_{en}}\right). \tag{5}$$

T_{en} is the period for all large bubbles rising up to the surface; U_B is the minimum terminal rise speed for the bubble group concerned, and $f\left(\frac{t}{T_{en}}\right)$ is the bubble accumulation function.

The breaking entrainment depth h_{en} can be written as

$$h_{en} = \frac{c_0^2}{g}\varphi\left(\frac{g}{\rho_w c_0^4}\frac{E_t}{S_t}\right). \tag{6}$$

where $\varphi(x)$ is an arbitrary function; and c_0, ρ_w, E_t and g are respectively characteristic wave speed, seawater density, mechanical energy loss and gravity acceleration.

Considering about the empirical forms of whitecap coverage in Eq. (1) and the relationship between whitecap coverage and entrainment depth, $\varphi(x)$ is obtained as

$$h_{en} = C_{en}\frac{c_0^2}{g}\left(\frac{g}{\rho_w c_0^4}\frac{E_t}{S_t}\right)^n, \tag{7}$$

where C_{en} and n are undetermined constants. Their values need be derived with whitecap observations. We substitute Eq. (7) into Eq. (4) to obtain

$$W = C_{en}F_T\frac{S_t}{U_B}\frac{c_0^2}{g}\left(\frac{g}{\rho_w c_0^4}\frac{E_t}{S_t}\right)^n. \tag{8}$$

In order to directly reflect the relationship between whitecap and wave characteristics, the equations of c_0, E_t and S_t in the paper of Yuan et al. (2009) are substituted in Eq. (8). By simplifying the equation, we can obtain

$$\begin{aligned} W = C_{en}F_T\frac{g^{0.5}\rho}{4\pi^{1.5}\alpha U_B}\left(\frac{\bar{L}}{\bar{\lambda}}\right)^{0.5}\times \\ \left[(1+\theta)\frac{\alpha^2\pi^2\lambda^2}{4\rho^2}\left(\frac{H_s}{\bar{L}}\right)^2\right]^n\times \\ \exp\left[-\frac{\rho^2}{2\alpha^2\pi^2\lambda^2}\left(\frac{L}{H_s}\right)^2\phi_0^2\right], \end{aligned} \tag{9}$$

where

$$\phi_0^2 = \left(1 - 0.55\,\frac{1}{\rho}\sqrt{2\pi\alpha\lambda C_D\,\frac{U_{10}^2}{g\bar{L}}}\right)^4, \tag{10}$$

$$\theta = \frac{g}{2\alpha\mu_4^{0.5}}\int_{-\infty}^{-\frac{g}{2\alpha\mu_4^{0.5}}\phi_0^2}\exp\left(-0.5Z^2\right)\mathrm{d}Z \times \exp\left(\frac{g^2}{8\alpha^2\mu_4}\,\phi_0^2\right). \tag{11}$$

Eqation (9) shows that whitecap coverage is related to the surface wind speed U_{10}, wavelength $\bar{L}$, wave slope $H_s/\bar{L}$ and ρ which is a parameter associated with wave spectrum width parameter. The value of , minimum terminal rise speed U_B, drag coefficient C_D and λ are separately 1, 0.25 m/s, 0.001 5 and 2/3, respectively.

3.2 *Improvement of the wave breaking model*

Although deriving the equation of whitecap coverage has made a great improvement, there could be some problems in the wave breaking model. We find that the coefficients of C_{en} and n obtain their value by choosing only two point of high wind speed on the upper envelope for all the whitecap coverage data. The method is not reasonable because the choice of the upper envelope and wind speed is not sufficient, which not only has subjective effect more or less but also could lead to over-estimates. So we need to search for more appropriate method to replace the old one.

The satellite-based parameterization can calculate W for the global area over a full year and consider the oceanographic and meteorological factors. The breaking wave model considers the bubbles with radii over 1 mm and the limit of foam thickness for satellite-based data in 37 GHz is around 1 mm, they both estimate whitecap coverage in active stage and residual stage. Therefore choosing the parameterization in Eq. (3) to derive the value of C_{en} and n is feasible.

Equation (9) can also be written as

$$W(X, Y, Z; C_{en}, n) = C_{en} Z X^n \exp Y, \tag{12}$$

where

$$X = (1+\theta)\,\frac{\alpha^2\pi^2\lambda^2}{4\rho^2}\left(\frac{Hs}{\bar{L}}\right)^2, \tag{13}$$

$$Y = -\frac{\rho^2}{2\alpha^2\pi^2\lambda^2}\left(\frac{\bar{L}}{H_s}\right)^2\phi_0^2, \tag{14}$$

$$Z = F_T\frac{g^{0.5}\rho}{4\pi^{1.5}\alpha U_B}\left(\frac{\bar{L}}{\lambda}\right)^{0.5}. \tag{15}$$

For a series of wind speed U_{10}, we can get arrays of *X, Y* and *Z* from Eq. (13) to Eq. (15) and get an array of *W* from Eq. (3). Thus the unknowns in the Eq. (12) are only C_{en} and n, and the least square method (LSM) can be applied to evaluate them.

4 Analyses and discussion

4.1 *Determining the appropriate constants and validating of the improved model*

Because U_{10}, wave slope $H_s/\bar{L}$ and ρ have influence on the whitecap coverage for Eq. (9), we take them as limiting conditions to evaluate the constants of C_{en} and n which are given in Table 2. It shows that the values of C_{en} and n change with different wave slope and wave spectrum width parameter.

For fully developed wave, ρ=0.577 4 and wave slope is above 0.082, the values of C_{en} and n are 1.542 9 and –1.546 6, which are consistent with the original constants C_{en}=1.44 and n=–1.557 4. It shows that the original model can only apply to fully developed wave. It may be related to the method by just choosing two points at high velocity and fitting the theoretical result with the upper-envelope curve. So we should obtain the constants of C_{en} and n for general wave state.

The relationships between whitecap coverage, wave slope and 10 m wind speed are shown in Fig. 2. When the wave slope is above 0.056, whitecap coverage is greater than zero, that is, the condition of wave breaking applies and whitecap appears. So it is reasonable to choose the values of C_{en} and n with this corresponding wave slope, and we obtain

$$C_{en} = 0.245\,1, n = -1.900\,6. \tag{17}$$

Moreover, based on the envelope for the whitecap data from Monahan (Monahan, 1971), Yuan et al. (2009) have obtained the constant C_{en}=0.2 and n=–1.89. Obviously, the result is nearly close to the new constants in Eq. (17).

In Fig. 2, whitecap coverage increases with greater wave slope. For most points with 5 m/s wind speed, whitecap coverage is nearly 0and wave slope is less than 0.055; for the points with 10 m/s wind speed, whitecap coverage is around 0.5%–1.5% and varies with wave slope; for the points with 15 m/s wind speed, the values of whitecap coverage and wave slope are greater than other two groups. So it illustrates that the model considers occurrence conditions of wave breaking and shows that high speed corresponds to high wave slope, promotes the breaking process and leads to more whitecaps.

Table 2. The constants of C_{en} and n under different limiting conditions

Limiting conditions				C_{en}	n
Wave state	U_{10}	H_s/L (above the value)	ρ		
General wave state	>5 m/s	0.050	0.35	0.147 6	–2.153 6
		0.051	0.35	0.136 7	–2.167 2
		0.052	0.35	0.140 5	–2.145 3
		0.053	0.35	0.156 0	–2.096 1
		0.054	0.35	0.177 1	–2.039 5
		0.055	0.35	0.217 7	–1.950 8
		0.056	0.35	0.245 1	–1.900 6
		0.057	0.35	0.291 0	–1.827 7
		0.058	0.35	0.347 2	–1.752 3
		0.059	0.35	0.413 1	–1.677 9
		0.060	0.35	0.489 4	–1.604 8
Fully developed wave	>15 m/s	0.082	0.577 4	1.542 9	–1.546 6

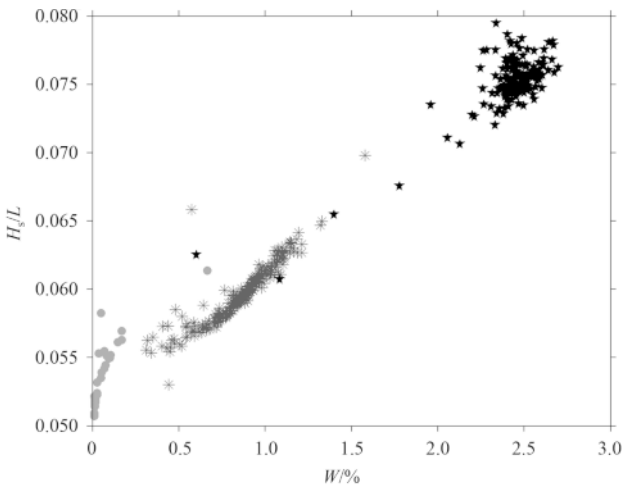

Fig. 2. Relationships between whitecap coverage, wave slope and 10 m wind speed. The dots, asterisks and stars represent the wind speed 5 m/s, 10 m/s and 15 m/s, respectively.

Global whitecap coverage for October 2006 is calculated by the wave breaking model in Fig. 3. By comparing the map of satellite-based data by Salisbury (2013, Fig. 2) and the results from the improved model, we find that both maps are generally similar except that simulated W in the model is a little higher in the western Pacific. Highest W occurs in bands centered around 50°S, which agrees with Sayer et al.'s (2010) statement. Most of the low-latitude and equator area, average whitecaps are less than 0.5%. The global average W is around 1.0%–3.0%, which is consistent with Blanchard's (1963, 1983) estimate ranging from 1.0% to 4.0%.

We compared the results which use the original constants and the new ones, respectively. Just considering the global distribution trends of whitecap coverage in Fig. 3, obvious differences are not witnessed in the two cases. It shows that different constants C_{en} and n have little influence on the geographic distribution trend of whitecaps. However, values of W in the original model are larger than those in the improved model by the factor of 3.0%–4.0% at high latitudes and 0.5%–1.0% at low latitudes. Estimates of original model are also larger than the satellite-based data. It indicates that the original constant C_{en} and n lead to larger simulated whitecaps and using the new constants is reasonable.

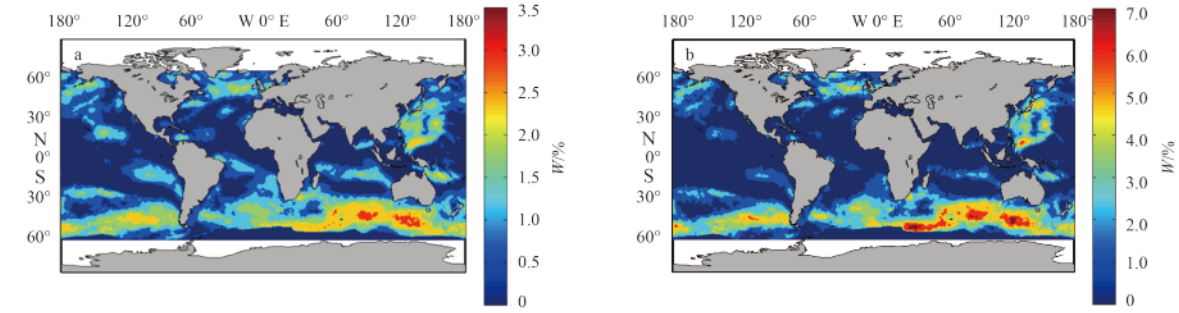

Fig. 3. Global whitecap coverage in October 2006 estimating by the improved model (a) and the original model (b).

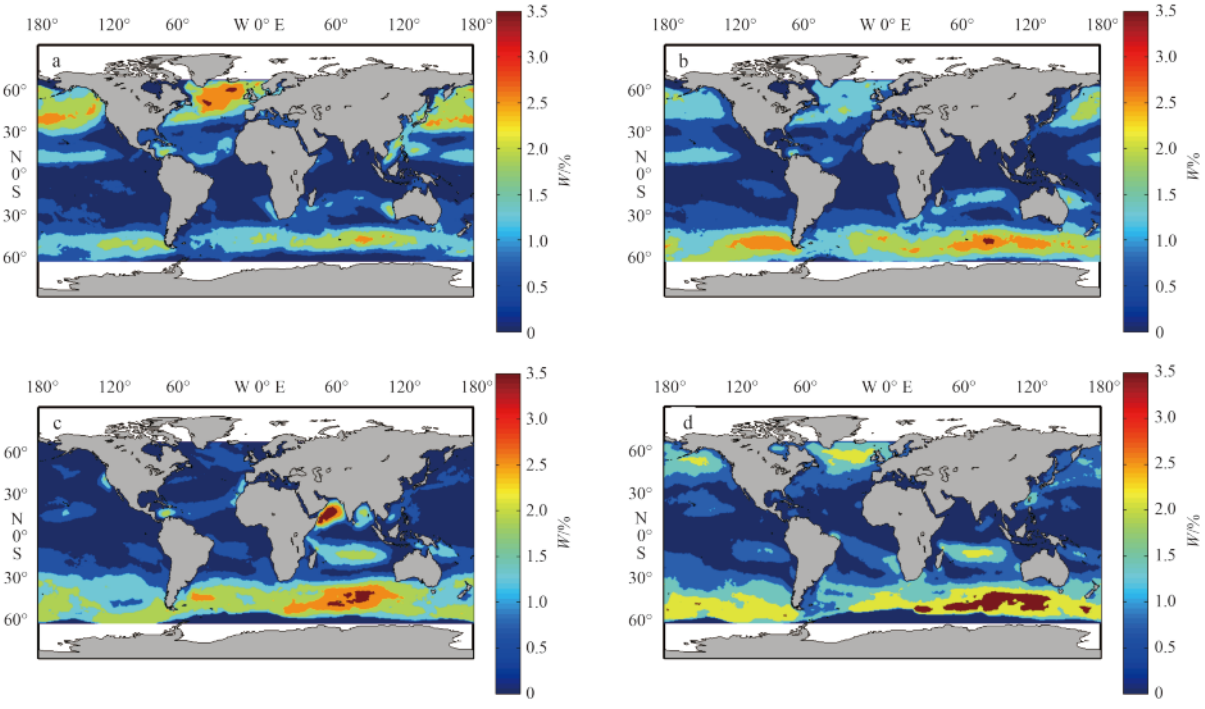

Fig. 4. Seasonal whitecap coverage in January (a), April (b), July (c) and October (d) which is average estimates from 1998 to 2008.

We can conclude that whitecap coverage estimated by the improved model is consistent with satellite-based data and observations from Monahan, which proves the reasonability of the new constants and whitecap coverage equation.

4.2 *Analysis of global seasonal whitecap coverage*

Global whitecap coverage from 1998 to 2008 is estimated by the improved model. The average W in the ten years is given in Fig. 4. It shows that there is a general trend of increasing W from the equator to high latitudes, and the difference of W between the both areas is at least 1.5%. Whitecap coverage is highest around 50°N and 50°S where seasonal variations are obvious, while the changes in the Northern Hemisphere are much stronger. At 50°–60°N, where W peaks, W is a factor of approximately 2% higher in January than in July. It shows that higher SST corresponds to lower whitecap coverage, that is, high SST could be against forming whitecap.

Whitecap coverage in the Northern Hemisphere is highest in January and W in the Southern Hemisphere is highest in October, compared with other three months. In July, W in the Northern Hemisphere is nearly less than 0.5%, while W in the Southern Hemisphere is almost above 1.5%. The result is in agreement with the statement of Blanchard (1963) and Erickson (1986). The asymmetric distribution of W is a consequence of the larger seasonal variations of wind and temperature in the Northern Hemisphere, where is driven by the stronger response of land surface temperature, and persistent high winds and long fetches in the Southern Hemisphere, both of which may result from the asymmetric distribution of land masses between the hemispheres.

5 Conclusions

Referring to the two methods of estimating whitecap coverage, parameterized empirical equations and the analytical statistical model, as stated in Sections 2 and 3, we analyze their advantages and disadvantages. Developed as the best fit to whitecap observations, parameterizations are simple and have abundant research achievements. However, there are wide variations from one parameterization to another, and they ignore the physical processes of forming whitecap. The model is based on surface wave dynamics with the effect of a wind drift layer. Whitecap equation in this model is a function of wave properties which imply an intrinsic dependence of whitecap coverage on the wave itself. But the method obtaining the value of constant C_{en} and n is not reasonable, which lead to over-estimates of whitecap.

Then we improve the analytical statistical model by applying the satellite-based parameterization to the model and using the least square method (LSM) to obtain multiple sets of constants C_{en} and n under different limiting conditions. The appropriate constants for general wave state are determined by considering the breaking condition of wave slope, which matches with the whitecap data from Monahan.

Comparing with satellite-based whitecaps and results from the original model, the improved model is validated to be more reasonable because its results are consistent with satellite-based whitecaps and agree with previous studies.

The global distribution and seasonal dependence of whitecap have been described. Whitecap coverage is highest around 50°N and 50°S, while the low-latitude and equator ocean, average whitecaps are less than 0.5% throughout the year. In the Northern Hemisphere, W is larger in winter than in summer, so is in the Southern Hemisphere. Seasonal changes at middle to high latitudes are stronger in the Northern Hemisphere than in the Southern Hemisphere.

An improved representation of the temporal and spatial distribution of whitecap will benefit parameterizations of air-sea interaction processes. Further study will be needed to develop workable and accurate proposals.

References

Anguelova M D, Gaiser P W. 2011. Skin depth at microwave frequencies of sea foam layers with vertical profile of void fraction. Journal of Geophysical Research: Oceans (1978–2012), 116(C11): doi: 10.1029/2011JC00737

Anguelova M D, Webster F. 2006. Whitecap coverage from satellite measurements: a first step toward modeling the variability of oceanic whitecaps. Journal of Geophysical Research: Oceans (1978–2012), 111(C3): doi: 10.1029/2005JC003158

Asher W E, Karle L M, Higgins B J, et al. 1996. The influence of bubble plumes on air-seawater gas transfer velocities. Journal of Geophysical Research: Oceans (1978–2012), 101(C5): 12027–12041

Asher W E, Wanninkhof R. 1998. The effect of bubble-mediated gas transfer on purposeful dual-gaseous tracer experiments. Journal of Geophysical Research: Oceans (1978–2012), 103(C5): 10555–10560

Blanchard D C. 1963. The electrification of the atmosphere by particles from bubbles in the sea. Progress in Oceanography, 1: 73, 113–112, 202

Blanchard D C. 1983. The production, distribution, and bacterial enrichment of the sea-salt aerosol. In: Liss P S, Slinn W N, eds. Air-Sea Exchange of Gases and Particles. Netherlands: Springer, 407–454

Callaghan A, de Leeuw G, Cohen L, et al. 2008. Relationship of oceanic whitecap coverage to wind speed and wind history. Geophysical Research Letters, 35(23): doi: 10.1029/2008GL036165

Callaghan A H, White M. 2009. Automated processing of sea surface images for the determination of whitecap coverage. Journal of Atmospheric and Oceanic Technology, 26(2): 383–394

Cardone V J. 1969. Specification of the Wind Distribution in the Marine Boundary Layer for Wave Forecasting (No. GSL-TR-69–1). New York: Cardone V J

de Leeuw G, Andreas E L, Anguelova M D, et al. 2011. Production flux of sea spray aerosol. Reviews of Geophysics, 49(2): doi: 10.1029/2010RG000349

Erickson Ⅲ D J, Merrill J T, Duce R A. 1986. Seasonal estimates of global oceanic whitecap coverage. Journal of Geophysical Research: Oceans (1978–2012), 91(C11): 12975–12977

Goddijn-Murphy L, Woolf D K, Callaghan A H. 2011. Parameterizations and algorithms for oceanic whitecap coverage. Journal of Physical Oceanography, 41(4): 742–756

Hanson J L, Phillips O M. 1999. Wind sea growth and dissipation in the open ocean. Journal of Physical Oceanography, 29(8): 1633–1648

Monahan E C. 1971. Oceanic whitecaps. Journal of Physical Oceanography, 1(2): 139–144

Monahan E C, O'Muircheartaigh I G. 1980. Optimal power-law description of oceanic whitecap coverage dependence on wind speed. Journal of Physical Oceanography, 10(12): 2094–2099

Monahan E C, O'Muircheartaigh I G. 1986. Whitecaps and the passive remote sensing of the ocean surface. International Journal of Remote Sensing, 7(5): 627–642

Monahan E C, Spillane M C. 1984. The role of oceanic whitecaps in air-sea gas exchange. In: Brutsaert W, Jirka G H, eds. Gas Transfer at Water Surfaces. Netherlands: Springer, 495–503

Monahan E C, Woolf D K. 1989. Comments on "Variations of whitecap coverage with wind stress and water temperature". Journal of Physical Oceanography, 19(5): 706–709

Salisbury D J, Anguelova M D, Brooks I M. 2013. On the variability of whitecap fraction using satellite-based observations. Journal of Geophysical Research: Oceans, 118(11): 6201–6222

Sayer A M, Thomas G E, Grainger R G. 2010. A sea surface reflectance model for (A) ATSR, and application to aerosol retrievals. Atmosphere Measurement Techniques, 3(4): 813–838

Stramska M, Petelski T. 2003. Observations of oceanic whitecaps in the north polar waters of the Atlantic. Journal of Geophysical Research: Oceans (1978–2012), 108(C3): doi: 10.1029/2002JC001321

Ulaby F T, Moore R K, Fung A K. 1981. Microwave Remote Sensing: Active and Passive. Volume 1-Microwave Remote Sensing Fundamentals and Radiometry. Reading, Mass: Addison-Wesley Publishing Company

Villarino R, Camps A, Vall-Ilossera M, et al. 2003. Sea foam effects on the brightness temperature at L-band. In: Proceedings of IEEE International Geoscience and Remote Sensing Symposium. Toulouse, France: IEEE, 5: 3076–3078

Wang Wei, Xu Delun, Lou Shunli. 1990. Directly synchronization measurement and results analysis of ocean whitecap and surface friction velocity. Haiyang Xuebao (in Chinese), 12(5): 638–647

Woolf D K. 2005. Parametrization of gas transfer velocities and sea-state-dependent wave breaking. Tellus: B, 57(2): 87–94

Wu Jin. 1988. Variations of whitecap coverage with wind stress and water temperature. Journal of Physical Oceanography, 18(10): 1448–1453

Yuan Yeli, Han Lei, Hua Feng, et al. 2009. The statistical theory of breaking entrainment depth and surface whitecap coverage of real sea waves. Journal of Physical Oceanography, 39(1): 143–161

Zhang Xin. 2012. Contribution to the global air-sea CO_2 exchange budget from asymmetric bubble-mediated gas transfer. Tellus: B, 64: doi: 10.3402/tellusb.v64i0.17260